

Original citation:

Ortega, Francisco J., Navarro, Francisco J., García-Morales, Moisés and McNally, Tony. (2017) Effect of shear processing on the linear viscoelastic behaviour and microstructure of bitumen/montmorillonite/MDI ternary composites. *Journal of Industrial and Engineering Chemistry*.

Permanent WRAP URL:

<http://wrap.warwick.ac.uk/84825>

Copyright and reuse:

The Warwick Research Archive Portal (WRAP) makes this work by researchers of the University of Warwick available open access under the following conditions. Copyright © and all moral rights to the version of the paper presented here belong to the individual author(s) and/or other copyright owners. To the extent reasonable and practicable the material made available in WRAP has been checked for eligibility before being made available.

Copies of full items can be used for personal research or study, educational, or not-for-profit purposes without prior permission or charge. Provided that the authors, title and full bibliographic details are credited, a hyperlink and/or URL is given for the original metadata page and the content is not changed in any way.

Publisher's statement:

© 2017, Elsevier. Licensed under the Creative Commons Attribution-NonCommercial-NoDerivatives 4.0 International <http://creativecommons.org/licenses/by-nc-nd/4.0/>

A note on versions:

The version presented here may differ from the published version or, version of record, if you wish to cite this item you are advised to consult the publisher's version. Please see the 'permanent WRAP URL' above for details on accessing the published version and note that access may require a subscription.

For more information, please contact the WRAP Team at: wrap@warwick.ac.uk

Accepted Manuscript

Title: Effect of shear processing on the linear viscoelastic behaviour and microstructure of bitumen/montmorillonite/MDI ternary composites

Author: <ce:author id="aut0005" author-id="S1226086X17300060-4f36759cb55ba066ecfb5a1f13867900"> Francisco J. Ortega<ce:author id="aut0010" orcid="0000-0002-8277-1073" author-id="S1226086X17300060-33cfe0c9d5c537178f20a446acfd05eb"> Francisco J. Navarro<ce:author id="aut0015" author-id="S1226086X17300060-5b52e3df441b49e50550689d6e7bc223"> Moisés García-Morales<ce:author id="aut0020" author-id="S1226086X17300060-ff4d040e0620c35497258c4e5653d909"> Tony McNally



PII: S1226-086X(17)30006-0
DOI: <http://dx.doi.org/doi:10.1016/j.jiec.2017.01.004>
Reference: JIEC 3248

To appear in:

Received date: 31-5-2016
Revised date: 3-1-2017
Accepted date: 3-1-2017

Please cite this article as: Francisco J.Ortega, Francisco J.Navarro, Moisés García-Morales, Tony McNally, Effect of shear processing on the linear viscoelastic behaviour and microstructure of bitumen/montmorillonite/MDI ternary composites, Journal of Industrial and Engineering Chemistry <http://dx.doi.org/10.1016/j.jiec.2017.01.004>

This is a PDF file of an unedited manuscript that has been accepted for publication. As a service to our customers we are providing this early version of the manuscript. The manuscript will undergo copyediting, typesetting, and review of the resulting proof before it is published in its final form. Please note that during the production process errors may be discovered which could affect the content, and all legal disclaimers that apply to the journal pertain.

**Effect of shear processing on the linear viscoelastic
behaviour and microstructure of
bitumen/montmorillonite/MDI ternary composites**

Francisco J. Ortega¹, Francisco J. Navarro¹✉, Moisés García-Morales¹, Tony McNally²

*¹Departamento de Ingeniería Química, Centro de Investigación en Tecnología de
Productos y Procesos Químicos (Pro²TecS), Campus de 'El Carmen', Universidad de
Huelva, 21071, Huelva (Spain)*

*²International Institute for Nanocomposites Manufacturing (IINM), WMG, University of
Warwick, CV4 7AL, Coventry (United Kingdom)*

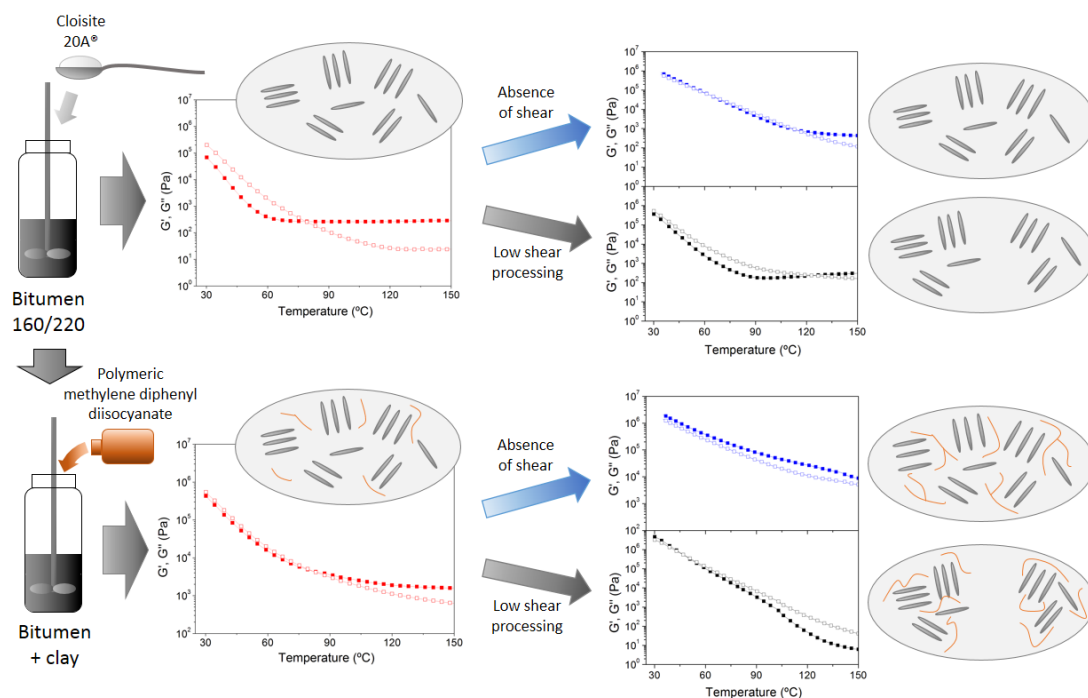
✉ Author to whom correspondence should be addressed:

E-mail: frando@uhu.es

Phone: +34 959218205

Fax: +34 959219983

Graphical abstract



ABSTRACT

Polymer modified bitumens (PMBs) have largely been utilized as a construction material. However, lack of affinity between bitumen and polymer leads to phase separation, and eventually, performance depletion. In this paper, alternative formulations of bitumen with an organically-modified montmorillonite (OMMT) Cloisite 20A® and polymeric methylene diphenyl diisocyanate (MDI) were prepared by melt blending. Their comprehensive rheological characterization evidenced improved linear viscoelastic properties when OMMT is added, revealing a noticeable structural reinforcement and thermal stability. Rheological data also showed that MDI-involved reactions control the composite end properties, being greatly influenced by the shear conditions applied.

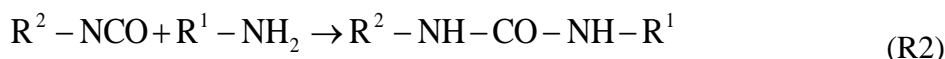
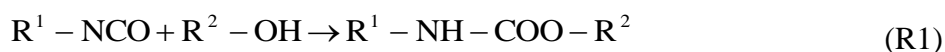
Keywords: bitumen, nanoclay, isocyanate, shear processing, composite

1. INTRODUCTION

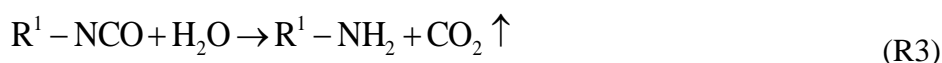
Bitumen has been largely used in the fields of pavement construction and roofing membrane manufacture. In this regard, its mechanical behaviour is highly influenced by the temperature, in such a way that, at low temperature, bitumen becomes fragile (thermal cracking), whilst at high temperature, it may undergo permanent deformation (rutting) [1]. Additionally, bitumen can also undergo ageing provoked by oxygen diffusion and UV radiation, which increases its thermal susceptibility and provoke premature fail [2,3].

Accordingly, bitumen has traditionally been modified by the use of different kinds of polymers, commonly copolymers like styrene-butadiene-styrene (SBS) and ethylene-vinyl acetate (EVA) which improve its mechanical performance by reducing the effective glass transition temperature and displacing the flow region to higher temperatures [4,5]. However, very often, the lack of affinity between polymer and bitumen results in an eventual phase separation at the macroscopic level with the consequent depletion in expected performance.

In this sense, some recent investigations have focused on the search for new bitumen modifiers. In particular, the use of reactive pre-polymers of functionalized polyols end capped with isocyanate groups have shown to be effective at noticeably enhancing bitumen properties [6–9]. As reported, these pre-polymers, with free -NCO groups, link to bitumen molecules containing active hydrogen groups (-OH and >NH) through urethane and urea covalent bonds, in accordance with reactions R1 and R2, respectively, in such a way that the size of the bitumen molecules/pre-polymer adducts continues to increase until there are no more -NCO groups available:



If water is present, it can also react with $-NCO$ groups, forming carbon dioxide as well as a highly reactive amine, according to reaction R3:



Next, this amine can further react with the remaining isocyanate groups following the above reaction R2. This set of reactions leads to the formation of larger molecules through urethane and urea linkages, giving rise to the development of more complex structures.

On the other hand, layered silicates (nanoclays) have recently attracted the interest of scientists in the polymer [10] and bitumen [11] fields, given their great potential for interactions at the nanometre scale. In particular, montmorillonite is a naturally occurring mineral mostly consisting of alumina-silicates with a layered structure, corresponding to sheets of silica tetrahedrons bonded to alumina octahedrons in a 2:1 ratio. In the interlayer space, inorganic cations are found to compensate the negative charge of the ions present in the silica-alumina layers. However, the inorganic nature of this cation leads to low compatibility when mixed with hydrophobic substances. Thus, ion-exchange reactions with quaternary ammonium salts with alkyl chains are required in order to render the nanoclay compatible with bitumen. Furthermore, a larger interlayer distance facilitates the insertion of the bitumen molecules in-between the layers during melt blending [3,12]. Depending on the extent of insertion, different

morphologies are distinguished (from poor to high quality): flocculated silicate platelets, intercalated and exfoliated structures [10,11,13].

The optimization of formulation/processing of nanocomposites with tailored properties requires a feedback process which includes their comprehensive rheological characterization [10,14]. In general, addition of clay to bitumen has yielded nanocomposites characterized by shear thinning behaviour at low shear rates, with noticeably increased viscosities with respect to their parent bitumen [3,11,13,15,16]. This has been attributed to hydroxylated edge-to-edge interactions between the dispersed nanoclay platelets [10,17], which tend to form an anisotropic continuum, disrupted by the application of large shear deformations [15]. In previous work with an organo-modified montmorillonite (Cloisite 20A®) [15,16], we reported a remarkable solid-like plateau which extended over a wide interval of high temperatures (100 – 165 °C) for a nanoclay concentration of 10 wt.%. However, further addition of 2 wt.% polymeric MDI, followed by 24 hours of curing, led to the disruption of the above structure and turned the solid-like plateau into a viscous flow region.

Accordingly, the main goal of the work described in this paper is to gain a deeper insight into the effects that an organo-modified montmorillonite (OMMT), by itself and combined with polymeric MDI, exerts on the thermo-rheological behaviour of the resulting bitumen composites under different shear conditions. Temperature-time sweep tests, chromatographic analysis (SARAs fractions) and modulated differential scanning calorimetry (MDSC) on bitumen/OMMT/polymeric MDI ternary formulations shed some light on the interactions involved.

2. EXPERIMENTAL

2.1. Materials

Composites were formulated using bitumen 160/220 as base material. Its specifications appear in Table 1, defined in terms of penetration degree (EN 1426:2007), softening temperature (EN 1427:2007) and composition, shown as “SARAs” fractions.

In addition to bitumen, formulations were prepared using the following additives as modifying agents:

- Cloisite® 20A (“C20A”, hereinafter), corresponds to a whitish, natural montmorillonite (MMT), organically modified with N,N-dimethyl di-hydrogenated tallow (C₁₄-C₁₈) quaternary ammonium cations in the interlayer space, characterised by a hydrogenated tallow consisting of a combination of octadecyl (65 wt.%), hexadecyl (30 wt.%) and tetradecyl (5 wt.%) groups. Besides the interlayer cations, MMT clays also contain hydroxyl groups on the edges of the platelets, which are liable to interact with other groups. Additional specifications: cation exchange capacity (CEC) of 92.6 meq/100 g clay, weight loss on ignition of 38 wt.%, moisture content lower than 2 wt.%, and according to X-Ray Diffraction, the interlayer distance is 2.42 nm. Platelets are approximately 1 nm in thickness, and the size distribution of dry platelets in their largest dimension ranges from values lower than 2 µm (10 vol.%) to lower than 13 µm (90 vol.%), with an average value of 8 µm, resulting in aspect ratios higher than 50.
- Polymeric MDI (4,4'-diphenylmethane diisocyanate), supplied by T.H. Tecnic (Spain), and characterised by an –NCO content of 30 wt.% [18]. It consists of an oligomeric mixture of 4,4'-diphenylmethane diisocyanate, 2,4' and 2,2' isomers, along with condensation products with more than two aromatic rings. Its typical composition contains approximately 50 wt.% pure MDI, 30 wt.% triisocyanate, 10 wt.% tetraisocyanate, 5 wt.% pentaisocyanate and 5 wt.% higher homologues.

2.2. Processing devices and sequence for bitumen modification

Two different processing devices were used depending upon the nature of the substances to be blended: for clay blending, a low-shear mixer, consisting of a 50 mm four-bladed impeller coupled to the blending device “IKA RW20”, which allowed processing at rotation speeds of 800 – 1000 rpm; and for polymeric MDI mixing, a high-shear mixer, based on the rotor-stator principle, composed of a dispersing accessory with a 25 mm diameter stator coupled to an “Ultraturrax™ T25 digital”, which reached rotation speeds ranging from 16000 to 18000 rpm. Both devices were purchased from IKA (Germany). Metal containers (109 mm diameter and 131 mm height), immersed into a bath with circulating oil, were used for the processing of samples.

The procedure of modification was applied according to the following sequence:

- 1) C20A pre-dispersion: 10 wt.%. C20A was progressively added to bitumen, previously heated up to 150°C, and stirred during approximately 10 min., using the low-shear mixing device, to ensure a homogeneous macroscopic dispersion. Afterwards, a part of the so-called “bitumen/C20A pre-dispersion” was used as such, whilst the rest was subjected to the following stage, part 2).
- 2) High shear blending (“HSB” in figure legends): the previous system was blended at high shear for 20 min. at 150°C, applying rotation speeds ranging from 18000 to 20000 rpm, in order to obtain a higher degree of dispersion. After this stage, the resulting “bitumen/C20A composite” was divided into three parts, so that one was used as such, another one subjected to low-shear mixing for 24 h, which resulted in the “24h-bitumen/C20A composite”; and the remaining part submitted to the next stage, part 3).

3) Reaction with MDI: 2 wt.% polymeric MDI was added to the composite and low-shear mixed at 150°C while curing for 1 h and 24 h (“1h-bitumen/C20A/MDI” and “24h-bitumen/C20A/MDI” composites, respectively).

In our previous results, the reactive interaction between –NCO in polymeric MDI and –OH in C20A was demonstrated, with a reaction mass ratio of 1.33 g of polymeric MDI per 10 g of C20A. Thus, for a formulation with 10 wt.% C20A, 2 wt.% polymeric MDI was added in order to ensure its reaction with the bituminous matrix, providing 2/3 –NCO for C20A and 1/3 –NCO excess. In relation to processing times, the properties of the resulting materials were evaluated after two different (short and long) curing periods (1 h and 24 h, respectively), envisaging a potential application.

Finally, any specific effect of the processing conditions on the resulting properties was also assessed by processing, according to the previous procedure, different blank samples of neat bitumen without modifiers.

2.3. Rheological Measurements and Material Characterisation

All the rheological tests were performed in a controlled-stress Physica MCR-301 rheometer (Anton Paar, Austria). Smooth plate-and-plate geometry of 25 mm in diameter, with 1-2 mm gap, was used for the entire set of samples. In every case, before testing, samples were equilibrated for at least 20 minutes at the test temperature.

Oscillatory-shear stress sweep tests were performed at a frequency of 1 rad/s, at temperatures ranging from 30 to 150 °C.

Oscillatory-shear frequency sweep tests were carried out at different temperatures ranging between 30 °C and the maximum possible value that allowed obtaining reliable

measurements. At each temperature, values of stress within the linear viscoelastic response were selected.

Oscillatory-shear temperature sweep tests, at a frequency of 10 rad/s, were carried out applying a heating ramp at a continuous rate of 1 K/min, from 30 °C up to the maximum possible temperature for reliability in the measurements. Moreover, in each case, strains were selected so as to ensure a linear viscoelastic response within the entire range of temperature tested.

Modulated differential scanning calorimetry (MDSC) was performed in a TA Q-100 (TA Instruments, USA) on 5 – 10 mg of sample inside hermetic pans. Every sample was submitted to the following procedure before testing, so that all of them were characterised by the same thermal history. Hence, initially, samples were heated up to 150 °C and left at that temperature for 30 minutes. Then, after a cooling period from the melt, they were annealed at room temperature for 24 h. Once annealed, a two-stage testing procedure was applied as follows, under nitrogen atmosphere. The first stage consisted on quenching to a temperature of -70 °C, keeping the sample at that thermal condition for 5 minutes. In the second stage, the temperature was risen at a rate of 5 K/min up to 150 °C in modulated mode, with a period of 60 s and an amplitude of 0.5 °C.

The compositional characterisation of bitumen was obtained by thin layer chromatography coupled with a flame ionization detector (TLC/FID), using an Iatroscan MK-6 analyser (Iatron Corporation Inc., Japan). Accordingly, the so-called “SARAs” fractions were eluted following the method outlined elsewhere [19], based on the sequential use of hexane, toluene and dicloromethane/methanol (95/5, by volume).

Every sample was subjected to testing at least three times in order to ensure the accuracy of the results obtained, which are shown as the average of the data gathered in each set of tests.

3. RESULTS AND DISCUSSION

3.1. Linear viscoelastic behaviour

In order to analyse general aspects of the effect that C20A and MDI addition exerts on the bitumen viscoelastic properties, Fig. 1A and 1B show the evolution of the complex modulus and loss tangent with temperature, at a constant frequency of 10 rad/s, for neat bitumen and, bitumen/C20A and bitumen/C20A/MDI composites, cured for 1 h and 24 h. For the sake of clarity, only one specific blank is presented (Blank 24h-curing), corresponding to neat bitumen with no additives, subjected to high shear blending and 24 h low shear stirring, because this is the only system that underwent a noticeable change in its thermo-mechanical properties. As depicted in Fig. 1A, neat and blank bitumen show steadily decreasing complex modulus values as temperature increases, with a dominating viscous response, according to the loss tangent values in Fig. 1B. The blank sample only shows a vertical shift of the curves (upwards for G^* and downwards for $\tan\delta$), pointing out a marked rise in stiffness, as a consequence of oxidative aging processes (“primary ageing”) that bitumen undergoes during processing at high temperature [1,6,8,20,21].

The addition of C20A to bitumen yields a considerable alteration of its viscoelastic behaviour. The complex modulus undergoes an increase of roughly one decade at around 30 °C (with respect to that of neat bitumen), showing a steady decrease with temperature up to a plateau of G^* , reached at approximately 105 °C. This plateau reveals a higher degree of thermal stability of the system structure, and hints at the

hypothesis related to the formation of some kind of reinforcing clay-based network, attributable to the intercalation/exfoliation of clay [15–17,22–24]. The loss tangent remains almost independent of temperature, with values barely greater than unity up to approximately 60°C, and then begins to steadily decrease as temperature was raised.

After MDI addition and 1 h curing, only minor changes were observed with respect to the bitumen/C20A composite up to 65 °C. Above that temperature, the system shows lower complex modulus values, and a plateau in G^* appears at approximately 130 °C. Analogously, the loss tangent exhibits values slightly higher than those of the bitumen/C20A system (Fig. 1B), pointing out that stirring during curing leads to a slightly less elastic sample.

After 24 h curing, the bitumen/C20A/MDI composite exhibited a markedly different behaviour. In the low temperature range, the complex modulus increased by two decades with respect to that of neat bitumen, maintaining a monotonic decrease in the entire temperature range examined. At higher temperatures, noticeable lower values than those corresponding to the rest of composites were obtained, seemingly attributable to the effects that the promotion of MDI-related reactive processes exert at longer curing times [7–9,25,26]. Fig. 1B also showed lower loss tangent values in the low temperature range, indicating a mostly elastic response, which rapidly becomes mainly viscous as temperature increases. It is also important to note that in the low temperature region (<50°C), the complex modulus of the bitumen blank (24 h curing) is similar to that of the bitumen/C20A and 1h-bitumen/C20A/MDI composites, clear indication that oxidation has some relevancy after 24 h high temperature processing.

In order to gain a deeper insight into the linear viscoelastic behaviour, Fig. 2 shows frequency sweep tests (G' and G'') carried out at several selected temperatures. As

shown, all the systems differ noticeably in their behaviour. The moduli of neat bitumen display the typical direct transition to the terminal flow zone, with a predominantly viscous behaviour in the entire range of applied frequency. The addition of C20A to bitumen yields a system with a mostly elastic response below the crossover frequency (~ 10 rad/s) at the lowest temperature (30 °C), shifting towards higher frequencies as test temperature increases, even disappearing at 90 °C. In correspondence with the temperature sweep data in Fig. 1, a rubbery “plateau-like” region seems to arise at low frequencies, indicating that the nanoclay is the main contributor to the linear viscoelastic rheology of the composite at temperatures at which bitumen softens, providing the material with an enhanced elastic response. Thereby, strong filler–filler interactions, as well as a high compatibility between C20A and bitumen play major roles in giving rise to a very highly-reinforced composite structure [22,27].

The addition of MDI to the previous composite and curing for 24 h provoked further changes in the linear viscoelastic functions. Hence, whereas at 30 °C the response is mainly elastic in the entire frequency range studied, with both curves nearly parallel; at higher temperatures, this behaviour turns predominantly viscous, leading to a remarkable drop in both moduli and, unlike the composite without MDI, the solid-like behaviour is no longer observed, just only a flattening of the low-frequency slopes.

As widely reported for composite materials [10,12–17,22–24,27–29], a better nanoclay dispersion yields an increase in interfacial area, allowing for optimal mechanical stress transfer between the filler and the matrix and, therefore, an enhancement in mechanical behaviour. In this regard, as discussed in previous works [15,16], the disappearance of the rubbery plateau region in the 24 h-bitumen/C20A/MDI composite has been attributed to the effects of MDI-related reactions under low shear processing, which, in fact, may promote the agglomeration/re-aggregation of C20A tactoids/platelets through

interactions between hydroxyl groups located on the edges of the clay platelets [10,12,15–17]. Moreover, in addition to the reactivity of –NCO groups in MDI with active hydrogen groups in bitumen, isocyanate groups can also react with pendant hydroxyl groups in C20A to form urea/urethane bonds [15], which may further contribute to the agglomeration of clay tactoids/platelets. As a consequence, large-sized aggregates containing new urea/urethane linkages would tend to form, reducing the degree of dispersion of clay platelets/tactoids, which causes the disruption of the clay-based reinforcing network, hence decreasing the bitumen/clay interfacial area, and so doing the strength of the material [12,15,16].

Fig. 3 depicts the phase angle versus the corresponding absolute value of the complex shear modulus from the dynamic rheological data (black diagram or Van Gorp–Palmen plot). These plots have been widely used not only for verifying the time–temperature superposition principle (TTS) in polymer blends and nanocomposites, but also for the evaluation of the topological structures in polymer-clay nanocomposites, given its sensitivity to structural or compositional changes [30].

Neat bitumen shows a well-known pattern consisting of a wide Newtonian viscous flow region at $G^* < 100$ Pa and a steady decrease of the phase angle at higher complex shear modulus values [20,31]. Only in the case of neat bitumen, all isothermal frequency data merge into a single common curve indicating that, at least empirically, the Time-Temperature-Superposition Principle holds.

The addition of C20A gives rise to a markedly different behaviour and a clear thermorheological complexity, which is further retained after MDI addition and curing for 1 h, as seen from the absence of superposition in the curves (Figs. 3b and 3c). The results reveal the greater contribution of the clay-related viscoelastic response to the overall

viscoelastic moduli when bitumen softens, given that the ranges of phase angle strongly shift towards low-to-intermediate values, indicating an increase in the elastic component of the system, especially at low frequencies (or high temperatures). Moreover, the flow region is not reached, and at temperatures higher than 60 °C, local minima clearly appear, for which the plateau modulus G_N^0 might be estimated [32], pointing to the presence of the rubbery plateau zone of the mechanical spectrum.

Increasing curing time up to 24 h led to the evolution of a completely different curve, as well as to the disappearance of the rubbery plateau zone. From 30 to 105 °C, the phase angle steadily diminishes as the complex modulus increases, reaching values of 10^7 Pa at 30 °C. At temperatures greater than 105°C, the curves tend to overlap, defining a maximum at a phase angle value of nearly 85°. This result indicates the material becomes less structured, displaying more liquid-like behaviour, and supports the structural destabilization previously stated.

In general, the observed rheological behaviour hints at the development of a complex, clay-based micro- and nano-structured continuum that reinforces the system structure and derives from the intercalation/exfoliation of clay tactoids in the bituminous matrix [14–16,23,24].

3.2. Linear and non-linear viscoelastic behaviour

Composites were also subjected to stress sweep tests, carried out in the temperature range from 30 to 150 °C, at 1 rad/s (Fig. 4). As reported in the literature [33,34], this type of oscillatory shear test is not only useful for determining the linear viscoelastic range (LVR), but also for obtaining valuable information about the material's microstructure. In this sense, the linear viscoelastic model states that both moduli lose physical significance when measured at stress values greater than the upper limit of the

linear viscoelastic range, since the output signal is no longer sinusoidal. However, the non-linear viscoelastic response is not substantially different from the moduli calculated by means of the linear viscoelastic equations and, therefore, can still be useful in providing relevant information about the microstructure of the system [33,35]. In this regard, different kinds of non-linear viscoelastic responses have been reported [33,34], which may be used to classify complex fluids, depending on the pattern traced by their non-linear viscoelastic functions: strain thinning (G' , G'' both decrease); strain hardening (G' , G'' both increase); weak strain overshoot (G' decrease, G'' increase followed by decrease); strong strain overshoot (G' , G'' both increase followed by decrease); as well as other intermediate behaviours.

Thereby, the resulting patterns for the viscoelastic moduli of the systems in this study, shown in Fig. 4, reveal a remarkable modification of the rheological response, especially in the non-linear regime, a fact that hints at morphological changes in the composites. In the case of the bitumen/C20A composite (Fig.4a), the linear viscoelastic range (at the lowest and highest temperature bounds considered) are both characterized by a predominantly elastic response, until a crossover shear stress value is reached. Beyond the critical stress, which sets the end of the LVR, the non-linear viscoelastic response arises as a steady decrease in both moduli (especially the elastic modulus), pointing out the stress thinning behaviour previously mentioned. This behaviour derives from the partial contributions of the bituminous matrix and C20A to the overall viscoelastic response. The presence of C20A, probably with a mostly-intercalated, hybrid structure [15,36,37], contributes to retain the elastic response over the viscous one, since it restricts the 'flowability' of the surrounding bitumen molecules [10,15,16,27,38,39]. Once the critical stress value is reached, the clay-based structural network is no longer stable, causing both moduli to start decreasing. The increase in the

test temperature reduces bitumen's partial contribution to the response, provoking a diminution in both dynamic moduli, widening the gap between them, as well as shifting the critical stress to a lower value.

By contrast, the viscoelastic response of the 1h and 24h-bitumen/C20A/MDI composites were more complex, as it depends on both the curing time and the test temperature (Fig. 4b). In the case of the 1 h-cured set of systems, a similar viscoelastic behaviour to that of the bitumen/C20A composite was observed. However, after being subjected to a longer curing time of 24 h, the viscoelastic response is noticeably modified. At low temperature (30 °C), the applied experimental stresses are not high enough to provoke a non-linear response, most probably due to the stiffening of the composite as a consequence of the reactions involving –NCO groups. As temperature was increased (≥ 80 °C), a completely different behaviour was observed. The viscoelastic response of the system turns predominantly viscous in the whole stress range applied, with a noticeably narrowing of the linear viscoelastic range, and upon exceeding the critical stress value, at 80°C, an intermediate non-linear response was obtained, with a local minimum in G' and G'' followed by a weak overshoot, to finally decrease again. At higher temperatures (130 and 150 °C, Fig. 4b), the viscoelastic response of the composite exhibits a remarkable stress thickening behaviour, represented by a rise of almost one order of magnitude in both moduli, followed by a decrease.

In this context, different types of structural network models have been proposed to predict and better understand the mechanism of strain hardening behind the non-linear viscoelastic response obtained. All consider the composite system structure to be represented by a network consisting of a combination of segments and junctions, whose distribution is dependent upon their rates of creation and loss. When both creation and

loss terms increase, but the speed of creation is slightly greater than that of destruction, a higher electrostatic interaction develops between the molecular chains in the system structure, which is eventually reinforced, showing a strong strain overshoot response in both viscoelastic moduli [33,34]. Therefore, in the case of the ternary system studied, when the complex molecular structure was subjected to dynamic oscillatory shear, intramolecular groups become available for intermolecular interaction with groups from other molecules in the structure, increasing the number of junctions and the effective volume occupied by the network [40]. The sum of these processes results in the observed increase in both viscoelastic moduli. However, as stress was increased, intermolecular junctions are progressively disrupted, leading to greater values of the loss rate parameter with respect to those of creation. Eventually, the network reaches such a degree of deformation that the intermolecular link distribution is unable to maintain the stability of the structure, giving rise to its collapse and the sudden decrease of both moduli [34,40], observed in Fig. 4b.

3.3. Effect of shear processing

With the aim of assessing the effect of shear during processing on the rheological properties of the composite systems, temperature sweep data collected for samples processed in a low shear mixing device for 24 h (as described in section 2.2) were compared to data recorded for samples of the same systems, which were instead subjected to a dynamic oscillatory shear testing protocol within the linear viscoelastic range, with an intermediate isothermal stage of duration and temperature comparable to those applied in the low-shear stirring procedure. This testing protocol consisted of a temperature sweep test in oscillatory shear from 30 to 150 °C (first stage), followed by an isothermal small-amplitude-oscillatory-shear (ISAOS) stage at 150 °C for 24 h, and finally, another temperature sweep from 150 °C down to 30 °C (third stage), as

portrayed in Fig. 5a, for the non-MDI-containing formulation; and Fig. 6a, for that containing MDI. Thermo-rheological data collected for each system after these two testing procedures are compared in Fig. 5b, in absence of MDI; and Fig. 6b, with MDI added to the formulation.

In Fig. 5a, the bitumen/C20A binary system (red pattern) is characterised by a mainly viscous response in the low-to-intermediate temperature range, with both moduli steadily decreasing down to a crossover point reached at 80 °C, and a rubbery plateau at higher temperatures. Once 150 °C was reached, the system was kept at that temperature in the LVE for 24 h (ISAOS stage), yielding a rise in both moduli, especially in G'' . This might be partially attributed to the previously mentioned effect of oxidation on the bituminous matrix. Nevertheless, given that the presence of nanoclay confers some protection against oxidation by hindering both the oxygen diffusion into bitumen and the release of volatile compounds [2,3], such a modification would mainly stem from structural changes in the extent of nanoclay dispersion. In fact, after the ISAOS stage, the temperature sweep data for the resulting system (blue pattern in Fig. 5a) shows a notable improvement in the linear viscoelastic response, with a rise in both moduli of approximately one decade over the entire temperature range, more intense in G' , and with the rubbery plateau appearing after a crossover, at approximately 110°C.

By contrast, when the bitumen/C20A system is low shear stirred for 24 h, the viscoelastic moduli did not only not improve, but actually slightly deteriorated, as shown in Fig. 5b (black pattern). The viscoelastic properties of the composite reveal a marked negative influence of the shear processing, since the system becomes predominantly viscous and the rubbery plateau almost vanishes.

Accordingly, these results suggest that the nanoclay intercalation/exfoliation process would be favoured at high temperature in the absence of stirring [28], probably allowing to achieve a higher degree of interaction between the bitumen matrix and nanoclay, which leads to such reinforcement of the system structure. However, under low shear stirring, the agglomeration/re-aggregation of clay tactoids would be promoted [12,15–17], yielding a higher presence of aggregates, accompanied by a lower degree of dispersion, and therefore, lower interaction between the clay and the bituminous matrix, which eventually decreases the structural reinforcement provided by the former.

In the case of the bitumen/C20A/MDI composites submitted to the same testing protocols, some differences can be found (Fig. 6a and Fig. 6b). As depicted in Fig. 6a, the system initially shows a crossover at intermediate temperatures, with G' slightly below G'' (red pattern in Fig. 6a). However, after the subsequent ISAOS stage at 150 °C for 24 h, the temperature sweep data from 150 to 30 °C (third stage) shows a notable increase in both moduli, with G' prevailing in the entire range of temperature (blue pattern in Fig. 6a). On the other hand, when the system was subjected to low shear stirring, a remarkable worsening of the linear viscoelastic behaviour was obtained (black pattern in Fig. 6b), still more pronounced than in the absence of MDI (black pattern in Fig. 5b). This brings about a notable shift of both moduli to lower values, with a viscous dominance of the LVE response, which is accompanied by the complete disappearance of the rubbery plateau.

Consequently, MDI content seems to further intensify the improvement derived from the intercalation/exfoliation of clay tactoids when no stirring is applied, which arises from the reactivity between isocyanate groups in MDI and active hydrogen groups, both in bitumen and C20A, yielding urea/urethane bonds [9,15,16,26], and a more complex, reinforced structure. By contrast, and similarly to the previous systems, shear

processing continues destabilizing the clay-based network, and its effect is now enhanced, as NCO-involved reactions seemingly promote the agglomeration/re-aggregation of clay tactoids/platelets, further reducing their degree of dispersion and the thermo-mechanical stability of the system structure.

It is also worth mentioning that data collected during the ISAOS stage in the dynamic oscillatory shear testing protocol provide some relevant information on the evolution of the LVE properties of both systems with time during 24 h at 150 °C, as depicted in Fig. 7. These data reflect the progress of chemical and physical processes behind the microstructural modification of the composites to reach the end properties. Accordingly, the variation observed in the moduli of the bitumen/C20A/MDI composite indicate that properties mainly develop within a time span of 4 h from the beginning of the ISAOS stage, and then slowly progress to reach roughly the final values after 18 h. In the case of the bitumen/C20A composite, G' remains practically unchanged over the entire curing period, whilst G'' increases slowly and steadily during the very same period of time. At the end of this stage, the values attained become the starting data of the following stage, as depicted in Figs. 5b and 6b. Therefore, in absence of reactive processes, the evolution of the properties merely results from physical interactions, as represented by data for the bitumen/C20A composite, which mainly arise from the initial high shear blending of C20A, with the ISAOS stage favouring aggregation processes that bring about an increase in the viscous modulus. By contrast, if reactive processes are also involved, curing during the ISAOS stage considerably affects the microstructure of the composite, and seemingly, no further relevant change is observed after 18 h. Hence, a steady state is approximately reached before 24 h curing, indicating that NCO-involving reactions proceed to such extent that their virtual completion can be assumed under the processing conditions applied.

3.4. Differential scanning calorimetry and chemical composition

The influence that the addition of clay and MDI to bitumen induces on its microstructure was also assessed by means of modulated differential scanning calorimetry (MDSC), a technique that allows investigation of the thermal behaviour of bitumen fractions, differentiating between reversing and non-reversing thermal events, like oxidation, evaporation or decomposition [41]. As depicted in Fig. 8a, four events can normally be distinguished in the non-reversing heat flow curve, as the different bituminous fractions order upon cooling from the melt: the first event, a broad endothermic background appearing from -60 to 90 °C; the second and third events, two exotherms usually centred at -15 °C and 40 °C, respectively; and the fourth event, an endotherm located at around 50 °C [42].

Thus, according to the data for the non-reversing heat flow enthalpies shown in Fig. 8b, the addition of clay provokes a marked change in the enthalpy of all the thermal events. The variation observed suggests that the molecular ordering of saturated segments that gives rise to cold crystallization (exotherms), as well as that related to the isotropization of resins and asphaltenes in an ordered amorphous phase (a mesophase) [41] are somewhat hindered, due to the molecular constraints that the intercalated/exfoliated clay tactoids exert on the mobility of the bitumen molecules [43].

Further addition of MDI and 1 h curing enhanced to a greater extent the hindering of molecular ordering, especially after 24 h curing, as deduced from the reduction in the enthalpy values for both cold crystallization exotherms [41] (second and third events in Fig. 8b). Moreover, MDI-related reactions contribute to form more complex molecular arrangements, which would raise the amorphous content, hence reducing the extent of ordering of the bitumen molecules [43,44].

As for the fourth event, this is related to the melting of slowly-ordered, high molecular weight compounds (mainly asphaltenes), in order to form mesophasic structures [42]. After 24 h curing, its value doubles to that of the 1 h-cured system, which may result from the combination of two effects. Firstly, oxidation processes that bitumen undergoes during shear processing at high temperature, which contribute to raise the asphaltene concentration in the system [1,6,8,20,21]. Second, the reported reactive interaction and linkage of $-NCO$ groups to active hydrogen groups in the most polar fractions of bitumen, which yields compounds with higher molecular weight [25], hence increasing the asphaltenic content.

In general, these results are consistent with the progressive formation of urea/urethane linkages between MDI, C20A and the most polar bituminous fractions. However, even though larger and more complex molecules are formed, the type of shear applied (small amplitude oscillatory shear or low shear stirring) determines if those new molecules contribute to a better nanoclay dispersion (see Fig. 6a) or tend to destabilise the system (see Fig. 6b).

Regarding the reversing component of the heat flow, data for its main contributor, the derivative of heat capacity [25], were also assessed (Fig. 9b). The peaks found in this signal arise from the glass transitions of the different amorphous phases present in bitumen (Fig. 9a). The glass transition temperature (T_g) depends on the stiffness, polarity, aromaticity and molecular weight of the molecules within the system, T_g increasing the greater the influence of these properties. In the case of the systems considered, four different peaks can be observed, exhibiting the characteristic pattern depicted in Fig. 9a. The first peak, located at -35 °C, is related to a phase rich in flexible paraffinic segments (saturates); the second, at around -5 °C, arises from the maltenic phase; the third peak is assumed to relate to an interfacial region with the presence of

mixed maltenes and asphaltenes, likely highly concentrated in resins. Finally, the fourth peak is associated with the asphaltenic phase [41,45].

As portrayed in Fig. 9b, after C20A addition, only T_{g3} is shifted towards a lower temperature, decreasing by approximately 7 °C. This variation in T_{g3} hints at some hurdle to the formation of the interfacial region between maltenes and asphaltenes. From the nano- up to micro-metre scale, the presence of intercalated/exfoliated clay tactoids hampers the interaction between asphaltenes and the surrounding molecules (mainly resins), reducing the presence of the former in the interphase. Hence, this region is enriched with maltenes, moving T_{g3} away from T_{g4} , which is associated with the asphaltenic fraction, leading to what can be regarded as a plasticizing effect [45].

The addition of MDI to the system, along with 1 h curing does not seem to modify the four glass transitions studied. However, increasing curing time up to 24 h gives rise to additional shifts in T_{g1} and T_{g2} , diminished by around 8 °C and 2 °C, respectively, with respect to those of neat bitumen. In this regard, the bitumen/clay/MDI molecular structural arrangements, formed as a result of the NCO-involved reactions, are assumed to possess enhanced relaxation dynamics, likely increasing the molecular dynamics of low molecular weight compounds, and consequently lowering the T_g 's results [46]. Moreover, as reactions proceed, the alignment and probable confinement of the molecular structures between the intercalated/exfoliated clay platelets might have also given rise to a lower degree of molecular density near the clay surface, thus, increasing the local free volume at the clay/bituminous matrix interface, as well as the amorphous fraction [43,46]. At longer curing times, the greater presence of these structural arrangements would also contribute to the hindrance of the ordering of certain bituminous fractions, as observed in the non-reversing heat flow thermal events (Fig. 8b).

Besides the studies described above, the so-called “SARAs” fractions (saturates, aromatics, resins and asphaltenes) were also assessed by means of thin layer chromatography (TLC/FID), in order to ascertain what influence C20A and MDI addition had on the chemical composition of bitumen and its microstructure.

As shown in Fig. 10 (values also included in Table 2), blanks point out that bitumen undergoes some oxidation during processing, also called “primary ageing”, by which aromatics are transformed into resins, and resins into asphaltenes [1,8]. Thereby, a slight decrease of around 5 wt.% was obtained in resins content, accompanied by a rise in asphaltenes of 4 wt.%. This oxidation tends to result in an increase in the values of the viscoelastic functions for bitumen, as observed in the rheological results, deteriorating its performance at low in-service temperatures [6,21].

When C20A was added to bitumen, a further evolution was clearly observed. The concentration of aromatics and resins decreased by nearly 5 and 7 wt.%, respectively, in favour of a rise in the asphaltenic fraction of around 10 wt.%. Apart from the contribution from certain oxidation, the variation obtained might result from the fact that the C20A cannot be eluted by any of the solvents employed in the chromatographic method used to separate the different bituminous fractions. Non-eluted C20A, in turn, may also interact with other compounds, especially high molecular weight molecules like those found in aromatics and resins, provoking their retention, and so lowering their concentration in the chromatographic separation in favour of the asphaltenic content.

As reported in the literature [47,48], it would be expected that the subsequent addition of MDI, followed by curing, led to a further similar modification of the system composition, i.e. a decrease in the aromatic fraction, along with a rise in the asphaltene content. However, the modification obtained is beyond that expected from

bitumen/MDI chemical interactions, since aromatics and resins markedly decrease, whilst asphaltenes rise by up to 32 wt.%, after 24 h curing. The evolution observed for the different fractions is mainly attributable to the reactive interaction of free –NCO groups in MDI with polar bitumen constituents, and with the hydroxyl groups that MMT clays naturally contain on the edge of the platelets [10,16]. The resulting modified bitumen compounds, with higher molecular weights, either inserted between the clay platelets or attached onto their surface, would not be eluted during the chromatographic separation, giving rise to the observed marked increase in asphaltene content [9,26]. This result points to the strong reactive interaction between the different constituents, yielding notable changes in the bituminous matrix microstructure and composition, in agreement with the results obtained from the rheological and thermal characterization.

4. CONCLUSIONS

The addition of 10 wt.% C20A to bitumen yielded a considerable alteration of the thermo-rheological behaviour with respect to those of neat bitumen, revealing a more thermally stable composite structure, manifest by the “rubbery” plateau-like zone defined by the viscoelastic functions, confirming the C20A was mostly intercalated within the bituminous matrix. The intercalated C20A facilitates the development of a more complex multiphase structural arrangement that acts as a reinforcing clay-based network, contributing to the retention of structural stability at temperatures at which bitumen normally softens.

Further addition of 2 wt.% MDI to the bitumen/C20A composite and 1 h curing led to a decrease in the global elasticity of the sample, accompanied by a small diminution of its thermo-mechanical behaviour, which has been attributed to the agglomeration/re-

aggregation of clay platelets/tactoids. Longer curing times provoked a marked change in the thermo-rheological response. First, oxidation processes of bitumen molecules led to increased asphaltenic fraction. Secondly, -NCO-involved reactions, which bring about the progressive formation of larger and more complex compounds containing urea/urethane linkages, further promoted the clustering of clay platelets/tactoids, destabilizing their reinforcing effect when the bituminous matrix softens, despite properties at medium in-service temperatures (30 – 40 °C) having been improved.

Moreover, the type of shear processing applied during curing has also been shown to greatly affect the composite system end properties, with clay intercalation/exfoliation processes being favoured in the absence of stirring, leading to a greater reinforcement of the system structure. Contrastingly shear processing promoted the re-aggregation of clay platelets/tactoids, diminishing their degree of dispersion, and therefore, the structural reinforcement provided by the clay. In the presence of MDI, processing shear effects were even more pronounced, as the –NCO-involved reactions determined whether new larger and more complex molecules contribute to a better nanoclay dispersion, if not stirred, or tended to destabilise the system, under shear processing.

Funding: This work is part of two research projects (CTQ2014-56980-R and TEP-6689) sponsored by a MINECO-FEDER Programme and the “Consejería de Innovación, Ciencia y Empresa, Junta de Andalucía” (“Projects of Excellence” Programme), respectively. The authors gratefully acknowledge their financial support.

Acknowledgements

References

- [1] J. Read,, D. Whiteoak, *The Shell bitumen handbook*, Fifth ed., Thomas Telford, London, 2003.
- [2] J.-Y. Yu,, P.-C. Feng,, H.-L. Zhang,, S.-P. Wu, *Constr. Build. Mater.* 23(7) (2009) 2636–40. 10.1016/j.conbuildmat.2009.01.007.
- [3] A. Zare-Shahabadi,, A. Shokuhfar,, S. Ebrahimi-Nejad, *Constr. Build. Mater.* 24(7) (2010) 1239–44. 10.1016/j.conbuildmat.2009.12.013.
- [4] F.J. Navarro,, P. Partal,, F. Martínez-Boza,, C. Valencia,, C. Gallegos, *Chem. Eng. J.* 89(1–3) (2002) 53–61. [http://dx.doi.org/10.1016/S1385-8947\(02\)00023-2](http://dx.doi.org/10.1016/S1385-8947(02)00023-2).
- [5] F.J. Navarro,, P. Partal,, F. Martínez-Boza,, C. Gallegos, *Fuel* 83(14–15) (2004) 2041–9. <http://dx.doi.org/10.1016/j.fuel.2004.04.003>.
- [6] F.J. Navarro,, P. Partal,, M. García-Morales,, M.J. Martín-Alfonso,, F. Martínez-Boza,, C. Gallegos,, J.C.M. Bordado,, A.C. Diogo, *J. Ind. Eng. Chem.* 15(4) (2009) 458–64. 10.1016/j.jiec.2009.01.003.
- [7] F.J. Navarro,, P. Partal,, M. García-Morales,, F.J. Martinez-Boza,, C. Gallegos, *Fuel* 86(15) (2007) 2291–9. <http://dx.doi.org/10.1016/j.fuel.2007.01.023>.
- [8] M.J. Martín-Alfonso,, P. Partal,, F.J. Navarro,, M. García-Morales,, C. Gallegos, *Eur. Polym. J.* 44(5) (2008) 1451–61. <http://dx.doi.org/10.1016/j.eurpolymj.2008.02.026>.

- [9] V. Carrera,, P. Partal,, M. García-Morales,, C. Gallegos,, A. Pérez-Lepe, Fuel Process. Technol. 91(9) (2010) 1139–45.
<http://dx.doi.org/10.1016/j.fuproc.2010.03.028>.
- [10] S. Sinha Ray,, M. Okamoto, Prog. Polym. Sci. 28(11) (2003) 1539–641.
[10.1016/j.progpolymsci.2003.08.002](http://dx.doi.org/10.1016/j.progpolymsci.2003.08.002).
- [11] G. Polacco,, P. Kříž,, S. Filippi,, J. Stastna,, D. Biondi,, L. Zanzotto, Eur. Polym. J. 44(11) (2008) 3512–21. [10.1016/j.eurpolymj.2008.08.032](http://dx.doi.org/10.1016/j.eurpolymj.2008.08.032).
- [12] K.N. Kim,, H. Kim,, J.W. Lee, Polym. Eng. Sci. 41(11) (2001) 1963–9.
[10.1002/pen.10892](http://dx.doi.org/10.1002/pen.10892).
- [13] S.G. Jahromi,, A. Khodaii, Constr. Build. Mater. 23(8) (2009) 2894–904.
[10.1016/j.conbuildmat.2009.02.027](http://dx.doi.org/10.1016/j.conbuildmat.2009.02.027).
- [14] S.T. Lim,, C.H. Lee,, H.J. Choi,, M.S. Jhon, J. Polym. Sci. Part B-Polymer Phys. 41(17) (2003) 2052–61. [10.1002/polb.10570](http://dx.doi.org/10.1002/polb.10570).
- [15] F.J. Ortega,, F.J. Navarro,, M. García-Morales,, T. McNally, Compos. Part B Eng. 76 (2015) 192–200. <http://dx.doi.org/10.1016/j.compositesb.2015.02.030>.
- [16] F.J. Ortega,, C. Roman,, F.J. Navarro,, M. García-Morales,, T. McNally, Fuel Process. Technol. 143 (2016) 195–203.
<http://dx.doi.org/10.1016/j.fuproc.2015.11.011>.
- [17] S.S. Ray,, K. Okamoto,, M. Okamoto, Macromolecules 36(7) (2003) 2355–67.
[10.1021/ma021728y](http://dx.doi.org/10.1021/ma021728y).
- [18] ASTM International, (2010). [10.1520/d2572-97r10](http://dx.doi.org/10.1520/d2572-97r10).

- [19] A. Eckert, *Pet. Coal* 43(3) (2001) 51–3.
- [20] D. Lesueur, *Adv. Colloid Interface Sci.* 145(1–2) (2009) 42–82.
<http://dx.doi.org/10.1016/j.cis.2008.08.011>.
- [21] A. Pérez-Lepe,, F.J. Martínez-Boza,, C. Gallegos,, O. González,, M.E. Muñoz,,
A. Santamaría, *Fuel* 82(11) (2003) 1339–48. [http://dx.doi.org/10.1016/S0016-2361\(03\)00065-6](http://dx.doi.org/10.1016/S0016-2361(03)00065-6).
- [22] A.K. Barick,, D.K. Tripathy, *Appl. Clay Sci.* 52(3) (2011) 312–21.
[10.1016/j.clay.2011.03.010](http://dx.doi.org/10.1016/j.clay.2011.03.010).
- [23] B. Hoffmann,, C. Dietrich,, R. Thomann,, C. Friedrich,, R. Mulhaupt, *Macromol. Rapid Commun.* 21(1) (2000) 57–61. [10.1002/\(sici\)1521-3927\(20000101\)21:1<57::aid-marc57>3.0.co;2-e](https://doi.org/10.1002/(sici)1521-3927(20000101)21:1<57::aid-marc57>3.0.co;2-e).
- [24] B. Hoffmann,, J. Kressler,, G. Stoppelmann,, C. Friedrich,, G.M. Kim, *Colloid Polym. Sci.* 278(7) (2000) 629–36. [10.1007/s003960000294](https://doi.org/10.1007/s003960000294).
- [25] F.J. Navarro,, P. Partal,, F. Martinez-Boza,, C. Gallegos,, J.C.M. Bordado,, A.C. Diogo, *Mech. Time-Dependent Mater.* 10(4) (2006) 347–59. [10.1007/s11043-007-9029-2](https://doi.org/10.1007/s11043-007-9029-2).
- [26] A.A. Cuadri,, M. García-Morales,, F.J. Navarro,, P. Partal, *Fuel* 118 (2014) 83–90. [10.1016/j.fuel.2013.10.068](https://doi.org/10.1016/j.fuel.2013.10.068).
- [27] K. Wang,, S. Liang,, J. Deng,, H. Yang,, Q. Zhang,, Q. Fu,, X. Dong,, D. Wang,,
C.C. Han, *Polymer (Guildf)*. 47(20) (2006) 7131–44.
[10.1016/j.polymer.2006.07.067](https://doi.org/10.1016/j.polymer.2006.07.067).

- [28] J.T. Yoon,, W.H. Jo,, M.S. Lee,, M.B. Ko, *Polymer (Guildf)*. 42(1) (2001) 329–36. 10.1016/s0032-3861(00)00333-5.
- [29] J. Yu,, X. Zeng,, S. Wu,, L. Wang,, G. Liu, *Mater. Sci. Eng. A* 447(1–2) (2007) 233–8. 10.1016/j.msea.2006.10.037.
- [30] M. Kracalik,, S. Laske,, A. Witschnigg,, C. Holzer, *Rheol. Acta* 50(11) (2011) 937–44. 10.1007/s00397-011-0545-2.
- [31] F. Merusi,, F. Giuliani,, G. Polacco, *Procedia - Soc. Behav. Sci.* 53 (2012) 335–45. 10.1016/j.sbspro.2012.09.885.
- [32] S. Trinkle,, C. Friedrich, *Rheol. Acta* 40(4) (2001) 322–8. 10.1007/s003970000137.
- [33] K. Hyun,, S.H. Kim,, K.H. Ahn,, S.J. Lee, *J. Nonnewton. Fluid Mech.* 107(1–3) (2002) 51–65. 10.1016/s0377-0257(02)00141-6.
- [34] H.G. Sim,, K.H. Ahn,, S.J. Lee, *J. Nonnewton. Fluid Mech.* 112(2–3) (2003) 237–50. 10.1016/s0377-0257(03)00102-2.
- [35] S.R. Raghavan,, S.A. Khan, *J. Colloid Interface Sci.* 185(1) (1997) 57–67. 10.1006/jcis.1996.4581.
- [36] R.A. Vaia,, E.P. Giannelis, *Macromolecules* 30(25) (1997) 8000–9. 10.1021/ma9603488.
- [37] R.A. Vaia,, K.D. Jandt,, E.J. Kramer,, E.P. Giannelis, *Chem. Mater.* 8(11) (1996) 2628–35. 10.1021/cm960102h.
- [38] V. Pryamitsyn,, V. Ganesan, *Macromolecules* 39(2) (2006) 844–56.

- 10.1021/ma051841z.
- [39] D. Wu,, C. Zhou,, W. Yu,, X. Fan, *J. Polym. Sci. Part B Polym. Phys.* 43(19) (2005) 2807–18. 10.1002/polb.20568.
- [40] V. Tirtaatmadja,, K.C. Tam,, R.D. Jenkins, *Macromolecules* 30(5) (1997) 1426–33. 10.1021/ma960098v.
- [41] J.F. Masson,, G.M. Polomark, *Thermochim. Acta* 374(2) (2001) 105–14.
[http://dx.doi.org/10.1016/S0040-6031\(01\)00478-6](http://dx.doi.org/10.1016/S0040-6031(01)00478-6).
- [42] J.F. Masson,, G.M. Polomark,, P. Collins, *Energy & Fuels* 16(2) (2002) 470–6.
10.1021/ef010233r.
- [43] P. Collins,, J.F. Masson,, G. Polomark, *Energy & Fuels* 20(3) (2006) 1266–8.
10.1021/ef050403q.
- [44] C.E. Corcione,, A. Maffezzoli, *Thermochim. Acta* 485(1–2) (2009) 43–8.
<http://dx.doi.org/10.1016/j.tca.2008.12.009>.
- [45] J.F. Masson,, G. Polomark,, P. Collins, *Thermochim. Acta* 436(1–2) (2005) 96–100. 10.1016/j.tca.2005.02.017.
- [46] S. Bandi,, D.A. Schiraldi, *Macromolecules* 39(19) (2006) 6537–45.
10.1021/ma0611826.
- [47] M.A. Izquierdo,, M. García-Morales,, F.J. Martínez-Boza,, F.J. Navarro, *Mater. Chem. Phys.* 146(3) (2014) 261–8.
<http://dx.doi.org/10.1016/j.matchemphys.2014.03.018>.
- [48] M.A. Izquierdo,, F.J. Navarro,, F.J. Martínez-Boza,, C. Gallegos, *J. Ind. Eng.*

Chem. 19(2) (2013) 704–11. 10.1016/j.jiec.2012.10.025.

Figure captions

Fig. 1. (a) Evolution of the complex modulus with temperature, and (b) evolution of the loss tangent with temperature, at 10 rad/s, for neat bitumen, and for bitumen/C20A and bitumen/C20A/MDI composites. Blank for high shear blending, followed by 24h stirring, is also included.

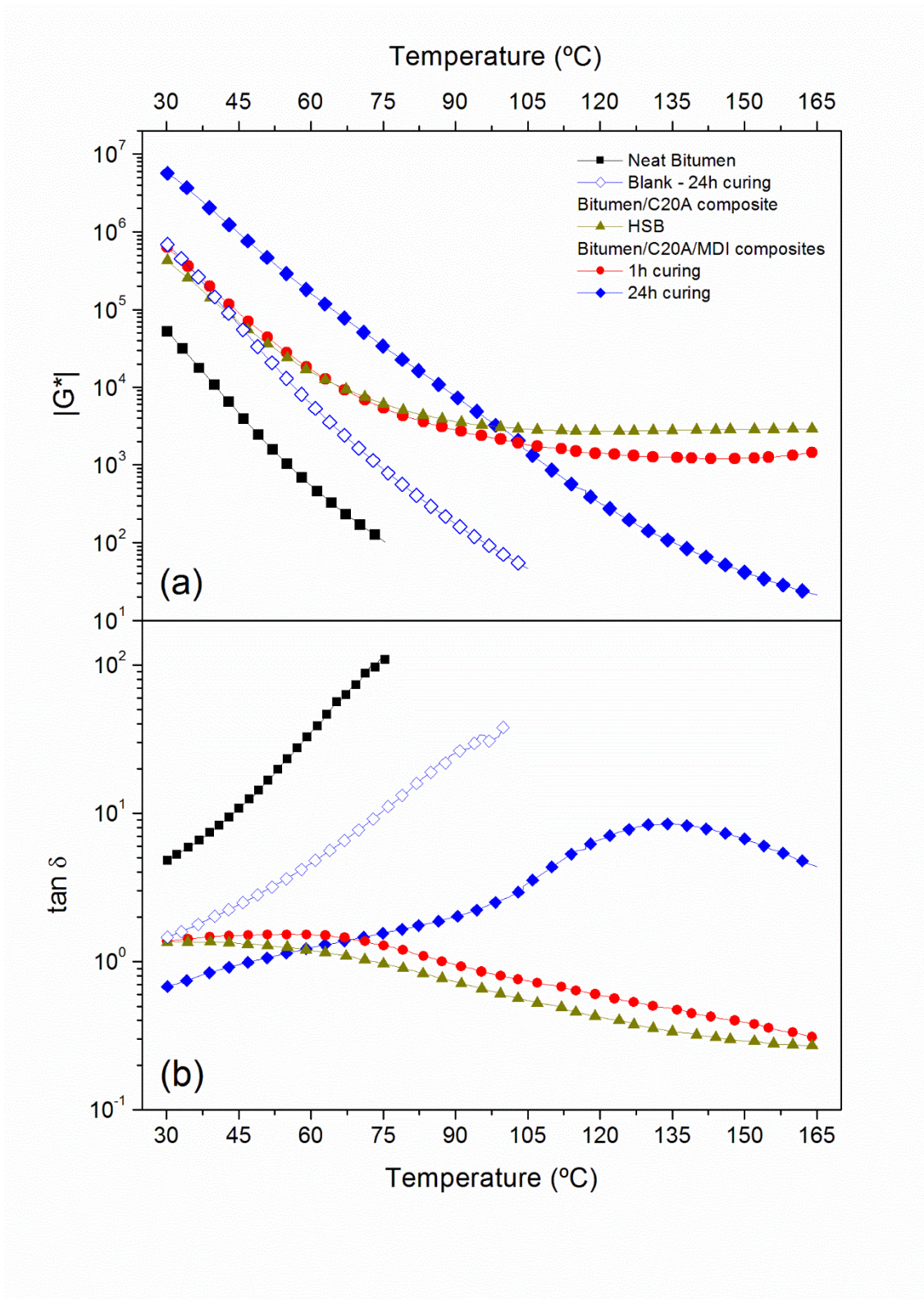


Fig. 2. Frequency sweep tests, at 10 rad/s, in the temperature range from 30 °C to 75 °C, with a step size of 15 °C between data series, for (a) neat bitumen; and from 30 °C to

150 °C, with a step size of 30 °C between data series, for **(b)** bitumen/C20A and **(c)** 24h-bitumen/C20A/MDI composites.

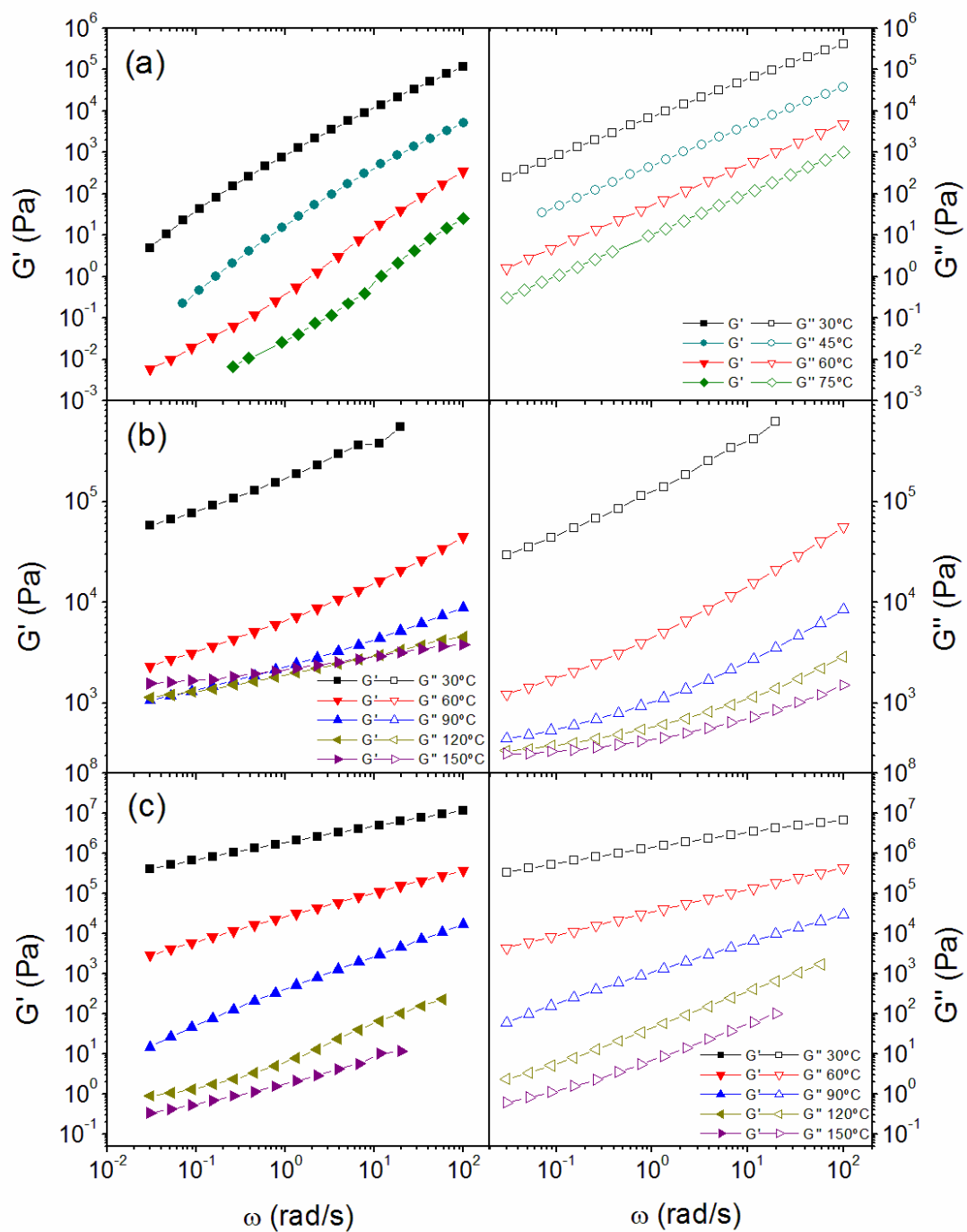


Fig. 3. Black diagrams, at 10 rad/s, with a step size of 15 °C between data series, for (a) neat bitumen, within the range of temperature from 30 °C to 75 °C; (b) bitumen/C20A composite, from 30 °C to 150 °C; and (c), (d) bitumen/C20A/MDI composites, from 30 °C to 150 °C.

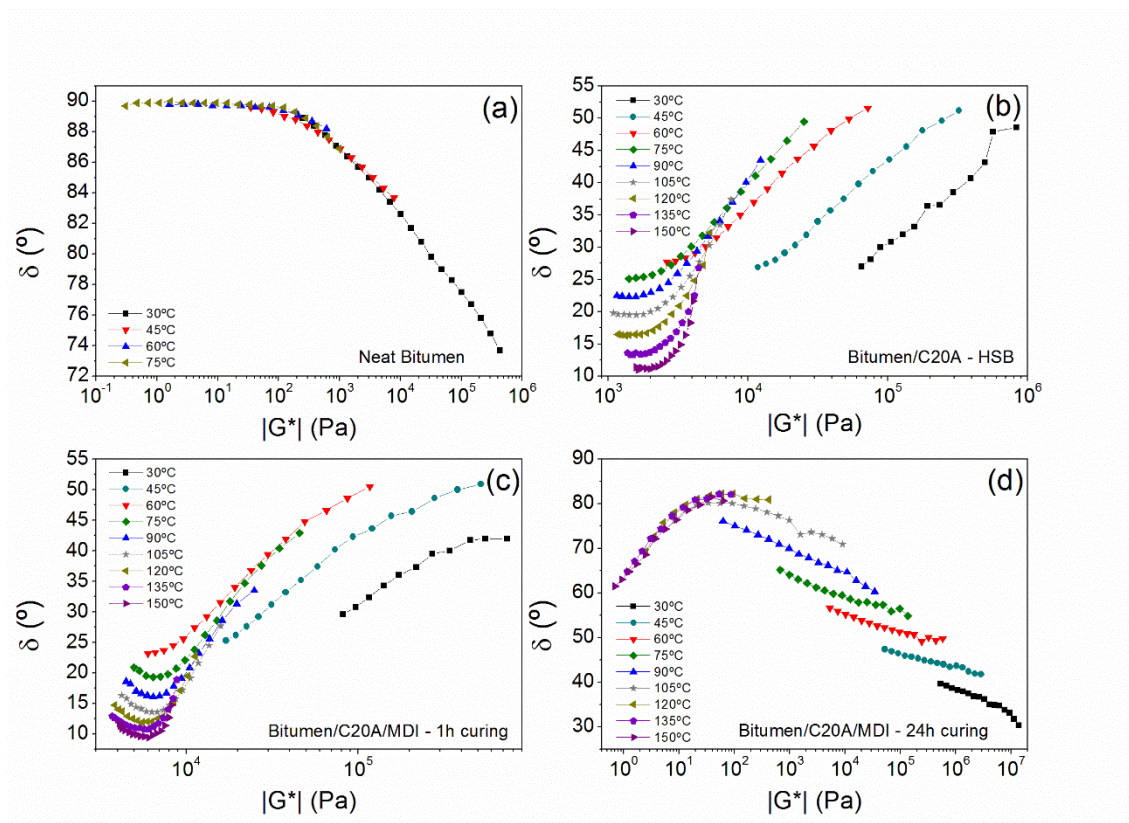


Fig. 4. Stress sweep tests, at 1 rad/s, for (a) bitumen/C20A composite, at 30 and 150 °C; and (b) bitumen/C20A/MDI composites at several temperatures between 30 and 150 °C.

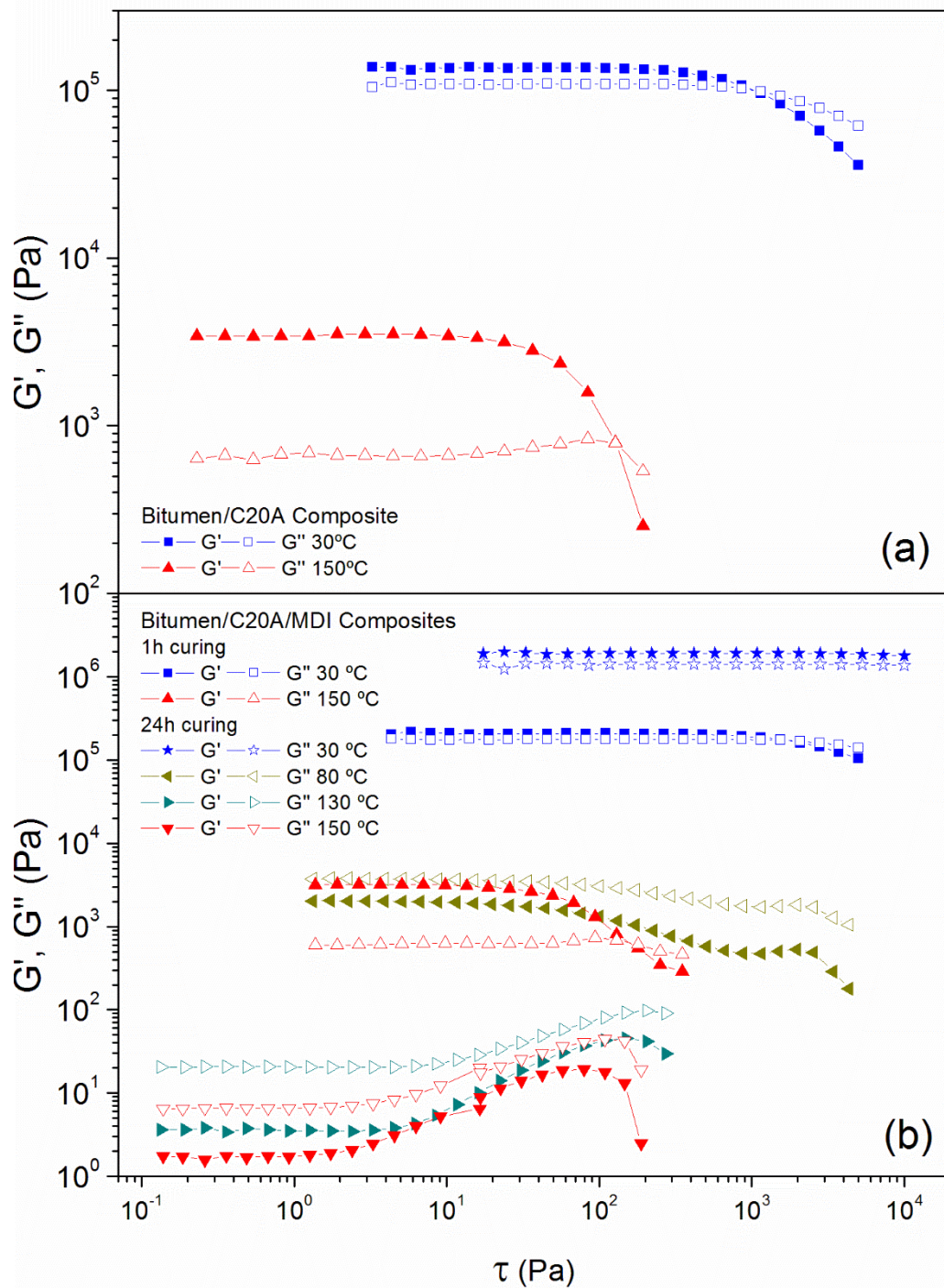


Fig. 5. Temperature sweep tests for bitumen/C20A composites: (a) dynamic oscillatory shear testing protocol within the linear viscoelastic range, with an intermediate isothermal stage at 150 °C for 24 h; and (b) temperature sweep patterns after shear

processing at 150 °C for 24 h (black pattern), and after the isothermal small-amplitude-oscillatory-shear (ISAOS) stage (blue pattern). Arrows point out the temperature ramp applied on each test.

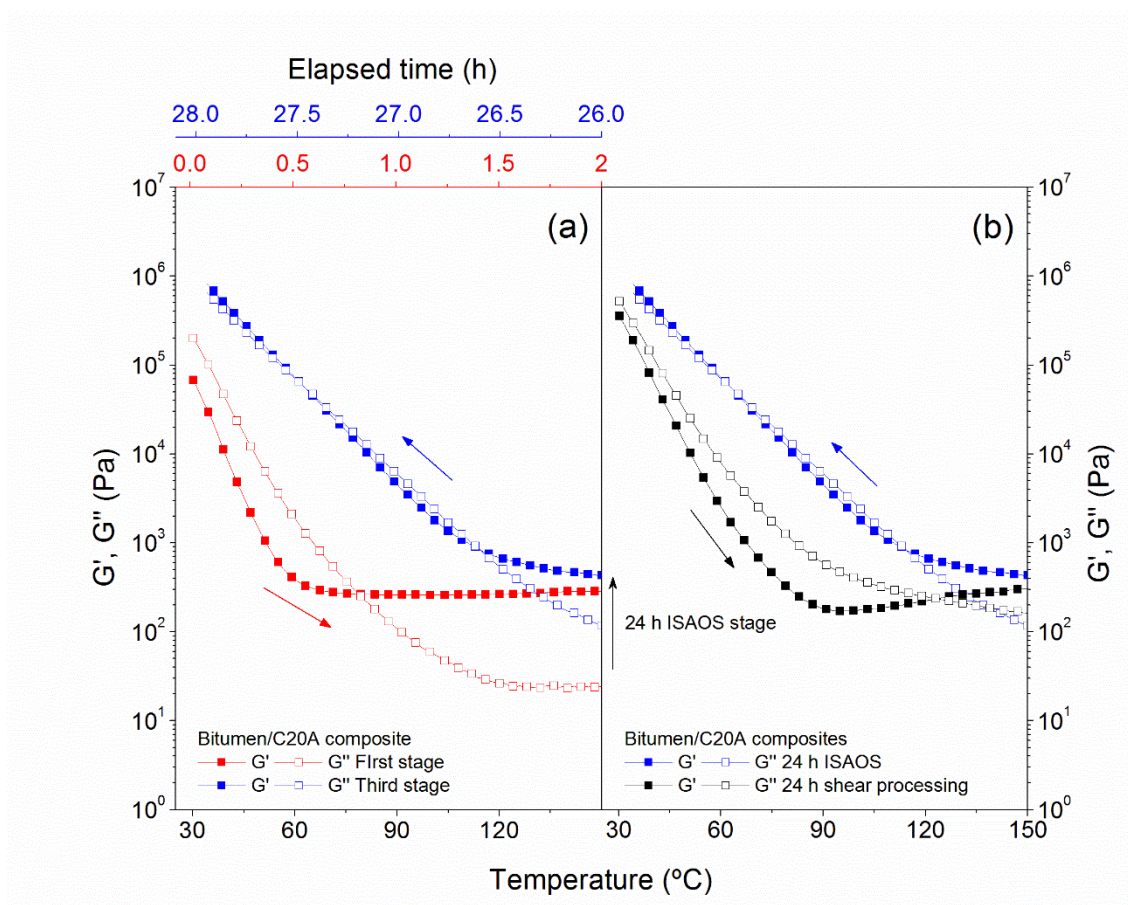


Fig. 6. Temperature sweep tests for bitumen/C20A/MDI composites: **(a)** dynamic oscillatory shear testing protocol within the linear viscoelastic range, with an intermediate isothermal stage at 150 °C for 24 h; and **(b)** temperature sweep patterns after shear processing at 150 °C for 24 h (black pattern), and after the isothermal small-amplitude-oscillatory-shear (ISAOS) stage (blue pattern). Arrows point out the temperature ramp applied on each test.

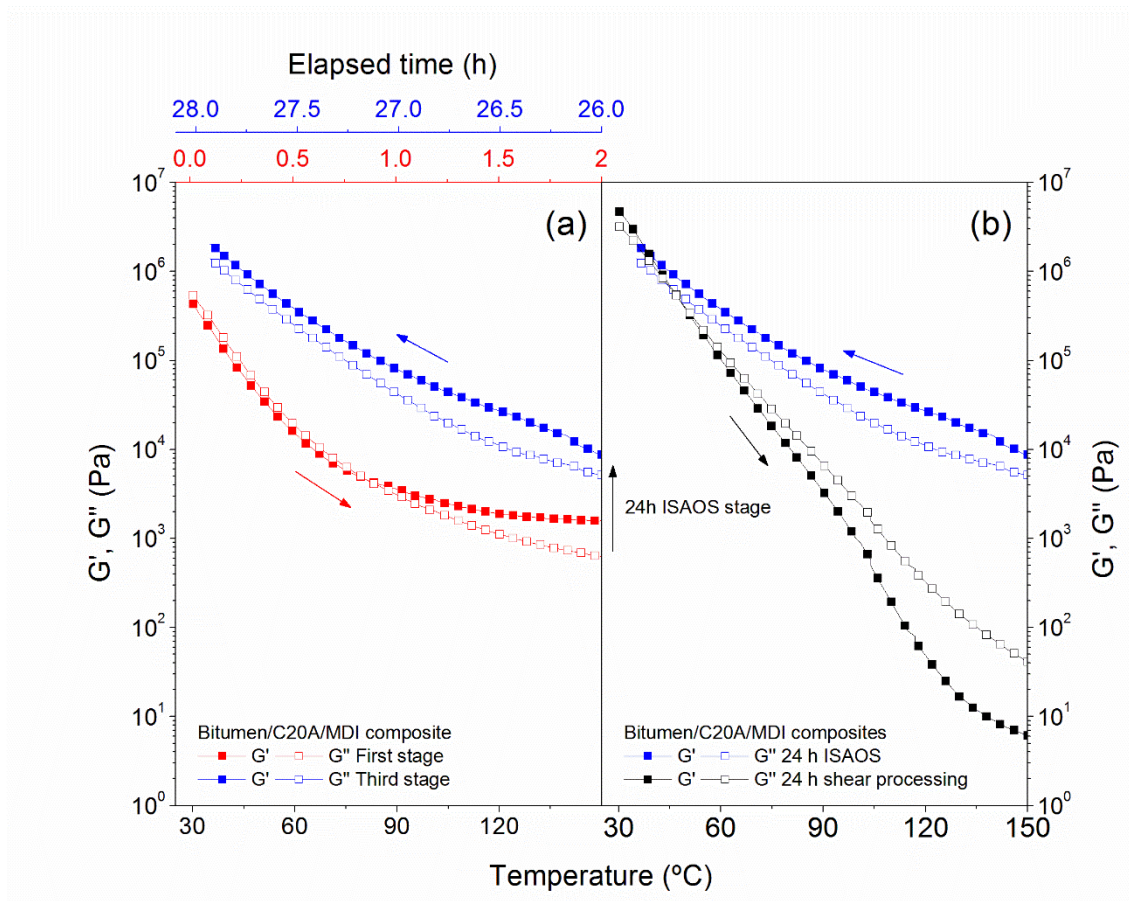


Fig. 7. Isothermal small-amplitude-oscillatory-shear (ISAOS) test at 150 $^{\circ}\text{C}$ for 24 h, for bitumen/C20A and bitumen/C20A/MDI composites.

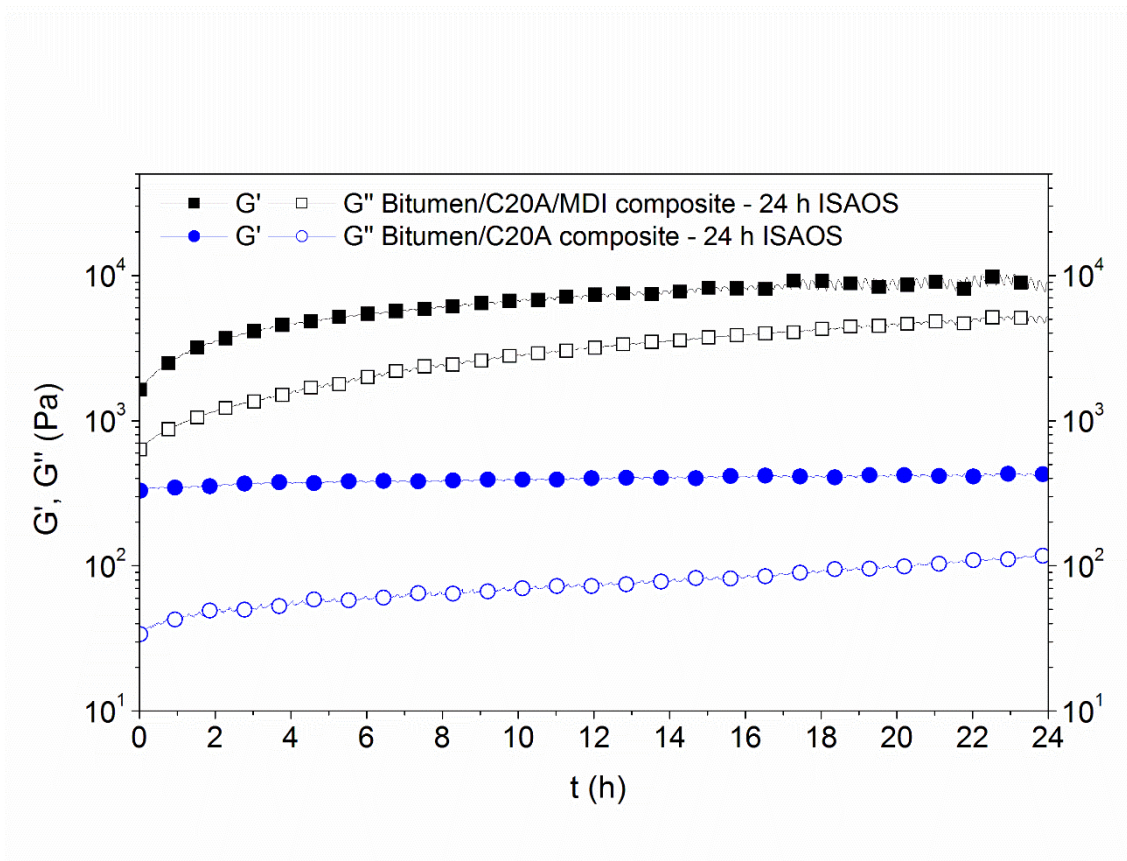


Fig. 8. (a) Typical pattern and thermal events for the non-reversing heat flow of the systems studied. **(b)** Enthalpy values of the non-reversing heat flow thermal events for neat bitumen, and for bitumen/C20A and bitumen/C20A/MDI composites.

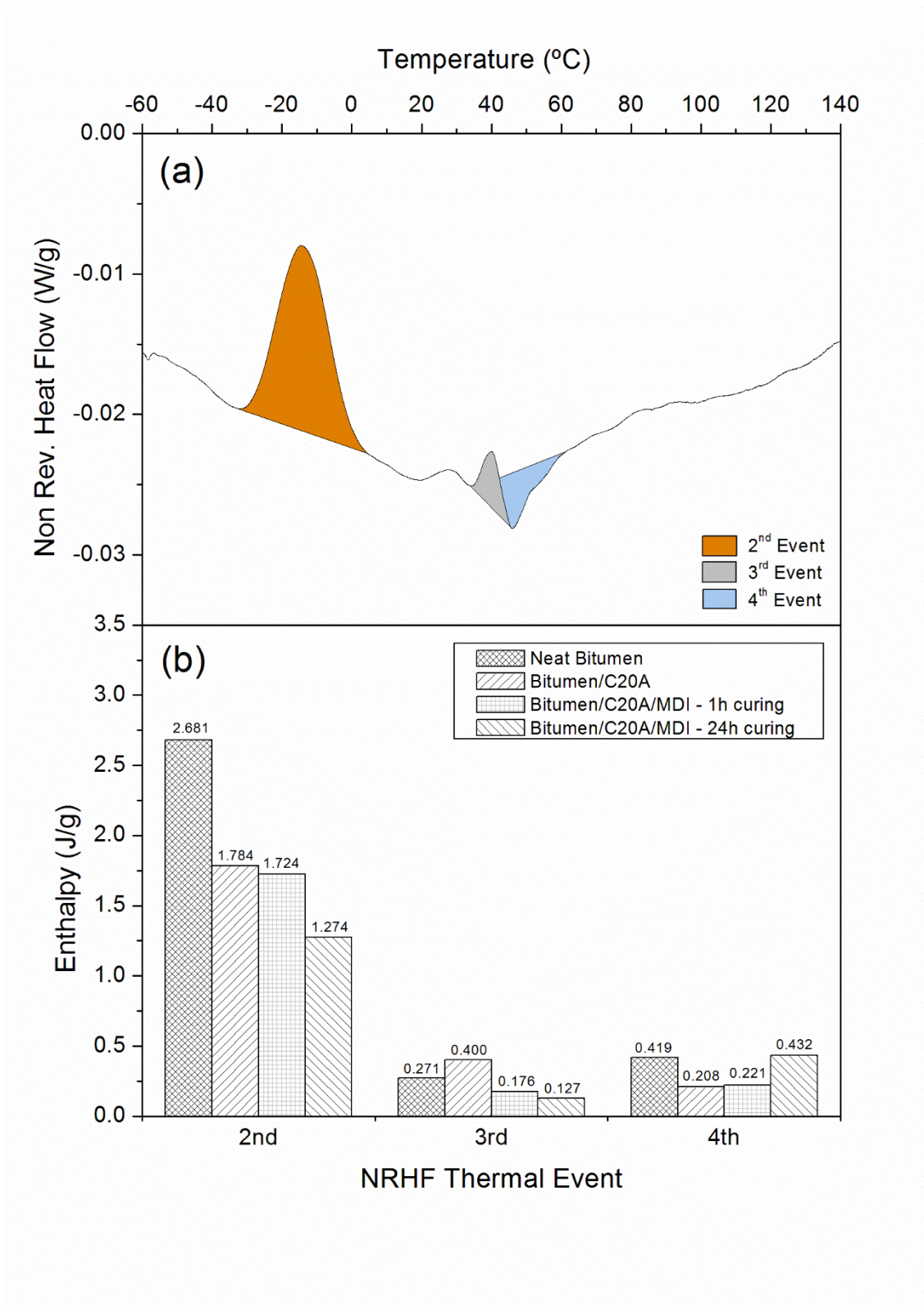


Fig. 9. (a) Characteristic pattern for the derivative of the heat capacity versus temperature for the systems studied, displaying the peaks corresponding to the different

T_g 's found. (b) T_g values for neat bitumen, and for bitumen/C20A and bitumen/C20A/MDI composites in the range of temperature from -60 °C to 150 °C.

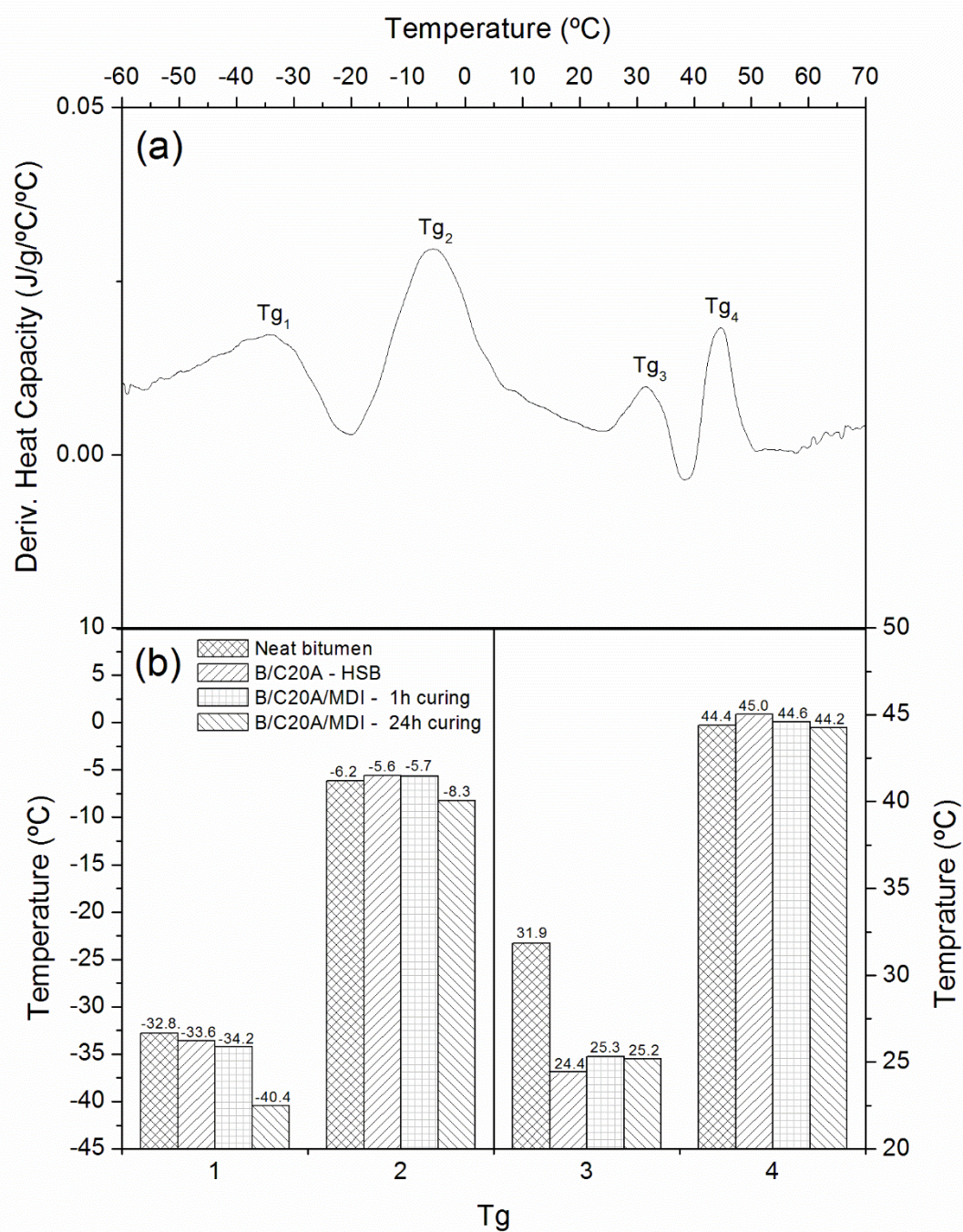


Fig. 10. Bitumen SARAs fractions for neat bitumen, and for bitumen/C20A and bitumen/C20A/MDI composites. Data for the corresponding blanks are also included.

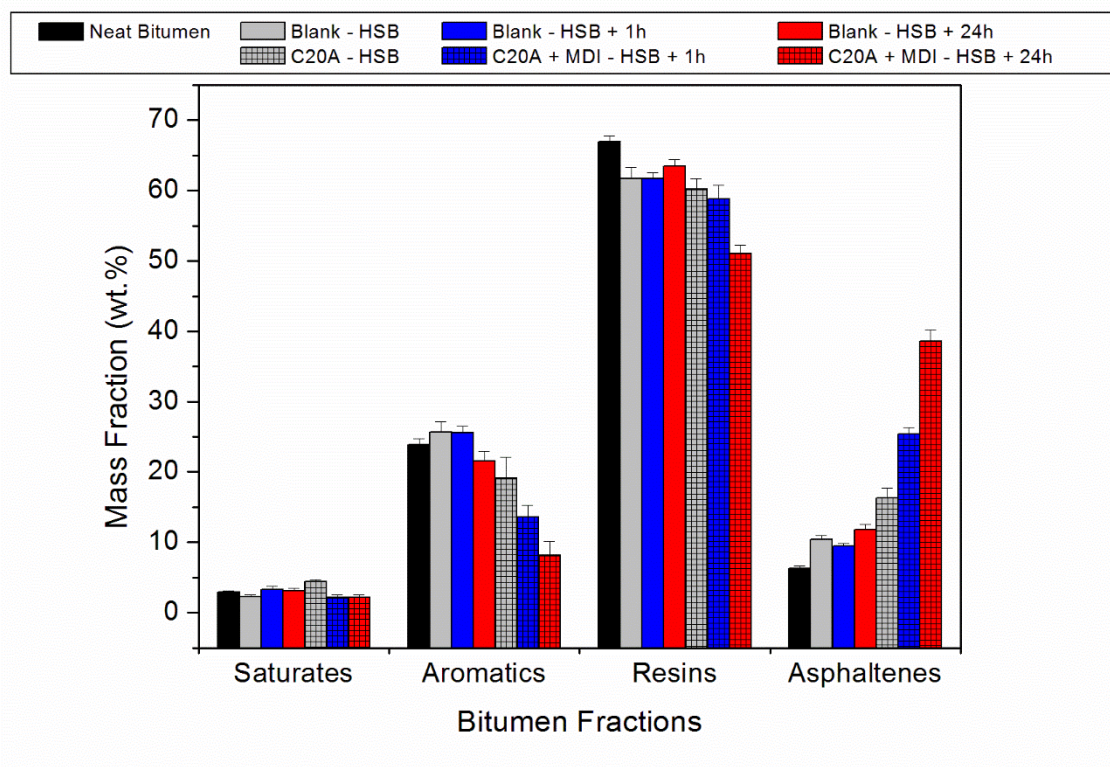


Table 1. Penetration, R&B softening temperature and composition (SARAs fractions) values for neat bitumen.

Specifications	Bitumen 160/220
Penetration (1/10 mm)	162
R&B softening point (°C)	42.4
Saturates (wt.%)	2.91 (0.21)*
Aromatics (wt.%)	23.84 (0.90)*
Resins (wt.%)	66.98 (0.83)*
Asphaltenes (wt.%)	6.27 (0.38)*

*Values given as mean (standard deviation)

Table 2. Bitumen SARAs fraction values for neat bitumen, and for Bitumen/C20A and Bitumen/C20A/MDI composites. Data for the corresponding blanks are also included.

Bituminous System	Saturates (wt.%)	Aromatics (wt.%)	Resins (wt.%)	Asphaltenes (wt.%)
Neat Bitumen	2.91 (0.21)	23.84 (0.90)	66.98 (0.83)	6.27 (0.38)
Blank - HSB	2.24 (0.32)	25.67 (1.49)	61.72 (1.58)	10.37 (0.55)
Blank - HSB + 1h curing	3.33 (0.46)	25.62 (0.87)	61.73 (0.82)	9.45 (0.36)
Blank - HSB + 24h curing	3.15 (0.33)	21.52 (1.39)	63.48 (0.93)	11.85 (0.71)
Bitumen/C20A - HSB -	4.43 (0.24)	19.08 (3.04)	60.17 (1.53)	16.31 (1.37)
Bitumen/C20A/MDI - HSB + 1h curing -	2.15 (0.38)	13.63 (1.68)	58.82 (1.93)	25.40 (0.94)
Bitumen/C20A/MDI - HSB + 24h curing -	2.17 (0.41)	8.15 (1.98)	51.06 (1.18)	38.62 (1.56)

Note: Values shown as mean (standard deviation).